Journal of Superconductivity and Novel Magnetism (2020) 33:3705–3715
https://doi.org/10.1007/s10948-020-05651-7

ORIGINAL PAPER

Fluctuation, Diamagnetic Transition, and FTIR Spectra of La Substituting Ca in (Bi,Pb):2223 Superconductor

A. Sedky[1] · Amna Salah[1]

Received: 1 February 2020 / Accepted: 21 August 2020 / Published online: 7 September 2020

Abstract

We report here fluctuation, diamagnetic transition, and FTIR spectra in $Bi_{1.7}Pb_{0.30}$ $Sr_2Ca_{2-x}La_xCu_3Oy$ superconductor with various x values ($0.00 \leq x \leq 0.30$). It is found that the magnetic moment is negative for the samples below the onset of diamagnetism in both field cooling (FC) and zero-field cooling (ZFC). Although the magnetic moments are shifted to lower values close to zero as La increases up to 0.30, they are higher for Fc than for ZFC. Furthermore, the onset temperature of diamagnetic transition (T_{cM}) for La = 0.30 sample is 83 K, which is about 30 K higher than that obtained from resistivity data (T_{cR} = 53 K). On the other hand, the logarithmic plots of excess conductivity $\Delta\sigma$ and reduced temperature ε for the samples reveal three different exponents corresponding to two crossover temperatures in the slope of each plot. The first exponent occurs in the normal field region (NFR) and its values are 0.30 (3D), 0.50 (3D), 0.20 (3D), and 2.04 (0D). The second exponent occurs in the mean field region (MFR) and its values are 0.75(2D), 0.44 (3D), 0.65 (2D), and 0.36 (3D). The third exponent occurs in the critical field region (CFR) and its values are 0.51 (3D), 0.99 (2D), 0.38 (3D), and 0.65 (2D). Interestingly, the Ginzburg-Landau parameter, critical magnetic fields, and critical current density are gradually increased as La increases up to 0.30, while the interlayer coupling, coherence lengths, anisotropy, and Ginzburg number are decreased. Finally, the FTIR absorption spectra of the samples show nine successive peaks due to O-H, Bi(Pb):2223, residual carbon, SrCo, $CaCo_3$ and CuO, and M-O, respectively. These results are discussed in terms of the correlation between hole carriers/Cu ions and excess oxygen which are introduced by La through CuO_2 planes of BSCCO superconductors.

PACS: 74.25.Bt74.62.Dh74.62.En74.72.gh

Keywords Excess conductivity · Diamagnetic behavior · Critical fields · FTIR spectra

1 Introduction

Due to short coherence length and high critical temperature T_c of superconducting materials, the thermal fluctuation of superconducting order parameter (Cooper pairs) has been early observed above T_c as excess conductivity [1, 2]. The fluctuation of Cooper pairs begins to be created spontaneously at a temperature twice the mean field temperature T_c^{mf} ($T \geq 2T_c^{mf}$) and normally increases as the temperature approaches T_c. The BSCCO high T_c superconducting systems have a layered structure in which two-dimensional conducting CuO_2 planes are separated by Bi charge reservoir layers, which impede the movement of charge carriers normal to the superconducting planes [3–9]. In particular, BSCCO exhibits anisotropy and small coherence length together with elevated values of T_c, and therefore, they have a great effect on superconducting order parameter [10–13].

The fluctuation-induced conductivity (FIC) analyses reveal that the contribution of excess conductivity is due to Gaussian fluctuation in the mean field region as well as the critical field fluctuation region [14]. Gaussian fluctuation is probably dominant in the temperature region above T_c^{mf} when the fluctuation in the order parameter is small and the interactions between Cooper pairs can be neglected, while the critical fluctuation occurs below the T_c^{mf} when the fluctuation in the order parameter is large and the interactions between Cooper pairs are considered. The variation of excess conductivity $\Delta\sigma$ with the reduced temperature ε helps the researches to find a lot of

✉ A. Sedky
sedky196000@hotmail.com

[1] Physics Department, Faculty of Science, Assiut University, Asyut, Egypt

superconducting parameters such as crossover temperature, dimensional exponent, interlayer coupling, coherence length, Ginzburg-Landau parameter, Ginzburg number, and anisotropy [15]. However, the dimensional exponents in high T_c materials are found to be zero dimensional (0D), one dimensional (1D), two dimensional (2D), and three dimensional (3D) [16, 17]. It seems that the dimensional crossover takes place between any two different dimension regions at a crossover temperature T_o.

The dimensional exponents of pure Bi(Pb):2223 systems are well described by 2D or quasi-2D nature [18–22]. They may also become 3D depending on the method of synthesis that modifies the state of microscopic disorder and induces spatial fluctuations near T_c.. Usually, the crossover can occur either from 3D to 2D or from 1D to 2D in the doped samples [23, 24]. While, the substitution of rare earth elements RE^{3+} at Ca^{2+} sites in these systems mutually has different dimensional exponents according to the changes of carrier concentration in the CuO_2 planes. For example, the substitution of Y, Pr, Ce, Gd, and Cd at Ca sites in Bi:2223 system suggests 2D superconducting order parameter, and a distinct 2D–3D crossover behavior near T_c is obtained [15, 25–30]. But the effects of La substitution on the above physical parameters such as critical fields and currents are not discussed in details.

The lattice vibrations in ceramic cuprates have been considered early as the subject of numerous studies and applications such as optical Kerr shutter (OKS), switching broadband amplifiers, detectors, and many other switching devices. Now, some evidences for electron-phonon coupling have been reported by infrared spectroscopy. The Fourier transform infrared (FTIR) spectroscopy has been early based on interference of radiation between two beams [31–34]. FTIR records the percentage of transmittance over a wide range of wavelengths like near infrared with frequency ranging 4000–10,000 cm^{-1}, middle infrared ranging 200–4000 cm^{-1}, and far infrared ranging 10–200 cm^{-1}. Therefore, in order to distinguish the different roles between the spin vacancy and the carrier concentration against substitution content such as La in Bi(Pb):2223 system, FTIR spectra (400–4000 cm^{-1}) are examined at room temperature.

Recently, Sedky et al. [35] have investigated the effect of La substitution on the structural, normal, and superconducting properties of $Bi_{1.7}Pb0_{0.30}$ $Sr_2Ca_{2-x}La_xCu_3Oy$ superconductors. The results of resistivity and Vickers hardness are presented in details. It is found that the replacement of Ca^{2+} by La^{3+} up to 0.30 increased the excess oxygen, effective Cu valance, hole carrier per Cu ion, and Vickers hardness H_v, and the T_c is decreased. Furthermore, the critical concentration for quenching superconductivity may be extended above 0.30. As a continuation of the above work, we reported here the fluctuation-induced excess conductivity on the same batch of samples. We have restricted our analysis to the mean field regime and crossover behavior and tried to extract some of the above important critical parameters. Furthermore, dc magnetization in both zero-field cooling (ZFC) and field cooling (FC) at dc magnetic field of 20 Oe is performed with the goal of establishing some evidence for the existence of local magnetic moments. Moreover, the FTIR spectra are taken in the frequency range of 400–4000 cm^{-1}.

2 Experimental

As indicated in ref. [36], the samples are synthesized by the well-known solid state reaction method and the structural, thermal, mechanical, and electrical properties are well examined in details. At present, and in order to determine the onset temperature of diamagnetism T_{cM} as well as critical temperature T_{cR} for the samples, dc magnetizations are carried out by means of a SQUID magnetometer (Quantum Design) in both field cooling (FC) and zero-field cooling (ZFC) at a field of 20 Oe in the temperature range of 10–150 K. More precisely, the samples are first cooled down to 20 K in the absence of the applied field; then, the field is switched on and the data are acquired for increasing temperature (ZFC) up to 150 K. After that, the samples are cooled down again and FC magnetization is acquired in the presence of the field. On the other hand, the FTIR absorption spectra of the samples are carried out in powder form in the range of 400 to 4000 cm^{-1} (with a resolution of 4 cm^{-1} and scanning speed 2 cm^{-1}/s at room temperature) using a spectrum 400-FT-1R/FT-NIR spectrometer. The samples are homogenized in spectroscopic grade of KBr carrier in an agate mortar and pressed in to 3-mm pellets. The grinding time is minimized as possible to avoid the structure deformation, ion exchange, and water absorption from the atmosphere.

3 Results and Discussion

It is evident from the XRD pattern shown in Fig. 1 that all samples are single phase and are free from any impurity phases. The peaks of high intensity indicated by H (hkl) belong to the Bi(Pb):2223 phase, while the peaks of very low intensity indicated by L (hkl) intensities such as (131), (115), (019) (240), (172), (310), and (3110) belong to Bi(Pb):2212 phase. However, the composition of low 2212 superconducting phase (T_c = 89 K) is normally formed as a minority phase in 2223 high phase, and cannot be considered as an impurity phase. Furthermore, these peaks have very low intensities as indicated above. The resistivity versus temperature curves for the samples are shown in Fig. 2. The critical temperatures T_{cR} for zero resistivity listed in Table 1 are 119 K for pure sample and decreased by La to 104, 71, and 53 K for La samples, respectively. Figure 3 a and b show the magnetic moment as a function of temperature in both zero-field

Table 1 T_{cR}, T_{cM}, average T_{cM}, ΔT_{cM}, and (T_{cR}–T_{cM}) versus La for pure and La samples

La cont.	T_{cR} (K)	T_{cM} FC (K)	T_{cM} ZFC (K)	Average T_{cM} (K)	ΔT_{cM} (K)	Temp. diff. (K)	d (Å)	c (Å)
0.00	119	112	114	113	2	6	18.436	36.872
0.05	104	91	87	89	4	15	18.408	36.816
0.15	71	82	–	82	–	11	18.389	36.778
0.30	53	87	79	83	8	30	18.384	36.768

cooling (ZFC) and field cooling (FC) for the samples. It is noted that the ZFC exhibits broader drop for the magnetic moment and extended from 20 K up to onset of diamagnetism, possibly due to a strong flux pinning effect, while the FC exhibits a sharp drop close to the onset of diamagnetism and nearly saturated as the temperature decreased to 20 K, indicating the presence of weak links. It is also noted that the magnetic moment is negative below the onset of diamagnetism for all samples in both FC and ZFC, but its value is higher for FC than that for ZFC. Furthermore, the magnetic moment is shifted to lower values close to zero as La increases up to 0.30.

Moreover, the clear difference in the superconducting signal coming from the ZFC curve, with respect to that of the FC curve, can be taken as proof that our ZFC protocol is correctly performed. The values of onset of diamagnetism T_{cM} for both cases are determined as the values of the temperature corresponding to the onset of the zero magnetic moment. As listed in Table 1, the average values T_{cM} between FC and ZFC are 113, 89, 82, and 83 K, and the temperature differences between them are between 2 and 8 K. As compared with the values of T_{cR}, the differences between the T_{cR} and T_{cM} values are 6, 15, 11, and 30 K, respectively. Although the diamagnetic signal is zero at this temperature, the area of the diamagnetic is higher than zero, indicating the presence of a superconducting state with a considered critical current [36, 37]. This observation suggests that the correct determination

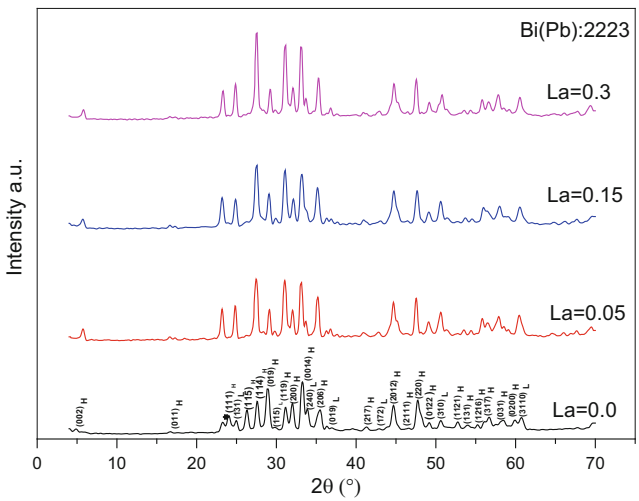

Fig. 1 XRD patterns for the samples

of T_{cM} is influenced by the presence of a magnetic background which overcomes the superconducting signal, particularly in the region close to the diamagnetic transition. However, the difference between T_{cR} and T_{cM} especially for La = 0.30 sample may be due to some of intrinsic inhomogeneities in superconductor which reflect two critical temperatures. The first is local temperature T_{cL} as a result of small clusters, and the other is percolation threshold temperature T_{cP} due to an infinite cluster giving a true zero resistance ($R = 0$). By using high-accuracy magnetic measurements, it is possible to determine the T_{cM} of the first islands due to pure clusters present essentially and appeared in the sample [38, 39].

The excess conductivity $\Delta\sigma$ due to thermal fluctuation is defined from the deviation of the measured conductivity σ_m (T) from the normal conductivity σ_n (T) as follows:

$$\Delta\sigma = \left(\frac{1}{\rho_m} - \frac{1}{\rho_n}\right) = \sigma_m - \sigma_n \quad (1)$$

where ρ_m and ρ_n are the measured and normal resistivity, respectively. ρ_n is obtained from the measured resistivity ρ_m at a temperature $T_B \sim 2\ T_c^{mf}$ by applying the least square method to the Anderson and Zou relation, $\rho_n(T) = A + BT$ [40]. In order to estimate the paraconductivity, Aslamazov and Larkin (AL) deduced the following relation for the fluctuation-induced excess conductivity $\Delta\sigma = A\varepsilon^{-\lambda}$ [41], where A is constant; λ is the order parameter exponent and their values are 2, 0.5, 1, and 1.5 for (0D/SW), 3D, 2D, and 1D fluctuations, respectively; and ε is the reduced temperature given by $\frac{T-T_c^{mf}}{T_c^{mf}}$ [40–42].

T_c^{mf} is the mean field temperature; above it, the interactions between Cooper pairs can be neglected. We have followed the dρ/dT versus temperature plot to obtain the values of T_c^{mf} from the peaks.

Here, $A = \frac{e^2}{32\hbar\xi_p(0)}$ for 3D, $A = \frac{e^2}{16\hbar d}$ for 2D, and $A = \frac{e^2\xi_c(0)}{32\hbar s}$ for 1D, e is the electronic charge, d is the interlayer spacing between any two successive planes, $\hbar$ is the reduced Planks' constant, $\xi_p(0)$ is the effective characteristic coherence length at 0 K, $\xi_c(0)$ is the c-axis 3D coherence length at zero temperature, s is the cross-sectional areas for 1D, and λ is an exponent related with the actual effective conduction dimensionality.

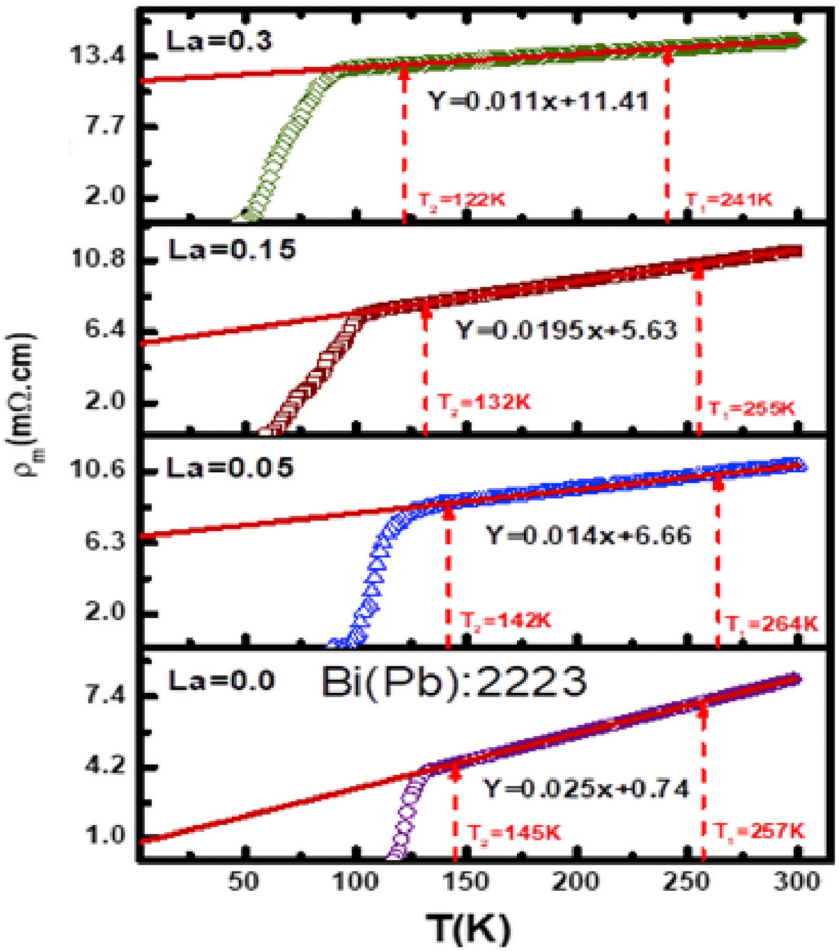

Fig. 2 Resistivity versus temperature for pure and La samples

The crossover behavior from 2D to 3D occurs at a temperature T_0, given by [42, 43]

$$T_0 = T_c^{\mathrm{mf}} \exp\left(\frac{2\xi_c(0)}{d}\right)^2 \tag{2}$$

where $\xi_c(0) = \left(\frac{dJ^2}{2}\right)$ [10, 44] and J is the interlayer coupling given by $J = \ln\left(\frac{T_0}{2T_c^{\mathrm{mf}}}\right)$ [45, 46].

The normal resistivity shown in Fig. 2 is found to be linear as the temperature is reduced from room temperature down to a certain temperature T_B, and follows the $\rho_n(T) = A + BT$ formula. $T_B \simeq 2T_c^{\mathrm{mf}}$ is the temperature below which the Cooper pair formation starts [47]. As the temperature is further reduced below T_B, the rate of change of resistivity becomes entirely different due to increasing Cooper pair formation. Therefore, the fluctuation-induced conductivity in this region follows the Aslamazov and Larkin (A-L) model to yield the dimensional exponent appropriate to fluctuation-induced conductivity [13].

However, ρ_n (T) is calculated by using the values of A and B parameters obtained from the fitting shown by straight columns in Fig. 2. One of the columns is drawn at a temperature close to T_B and the second drawn at a temperature very close to room temperature. The mean field temperature T_c^{mf}, listed in Table 2, is estimated from the peak of dρ/dT against temperature plot as shown in Fig. 4. By using the values of $\Delta\sigma$ and reduced temperatures ϵ, we have plotted $\ln\Delta\sigma$ against $\ln\epsilon$ for all samples (see Fig. 5). Evidently, above T_c^{mf}, we first observe a power law region which clearly means that the G-L theory breaks and the short wave fluctuation play a dominant role [48]. Also, the excess conductivity decreases sharply in this temperature region and agrees well with the theoretical prediction. However, three distinct linear parts are obtained for each curve. The first part occurs in the normal field region (NFR), the second in the mean field region (MFR), and the third in the critical field region (CFR). The corresponding temperatures where the slope change occurs are designated as the crossover temperatures T_{o1} and T_{o2}, respectively. The values of T_c^{mf} T_{o1} and T_{o2} listed in Table 2 are decreased as La increases up to 0.30 as well as T_{cR} behavior. The interlayer coupling J is calculated in terms of T_c^{mf} and T_{o2} values, and then, $\xi_c(0)$ could be also obtained, in which $d = c/2$ for BSCCO systems [49]. It is clear that both of J and $\xi_c(0)$ are decreased as La increases up to 0.30 as well as c-axis.

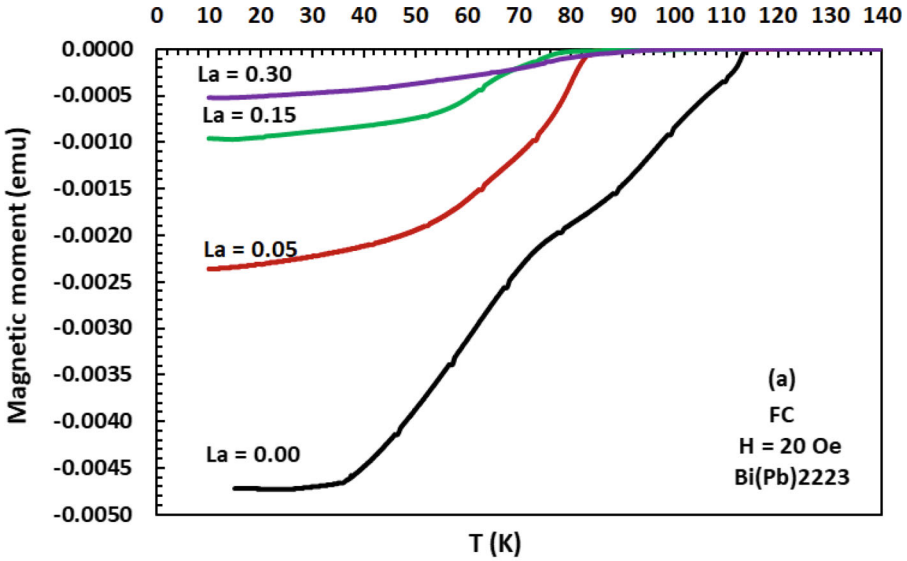

Fig. 3 **a** The FC magnetic moment versus temperature for pure and La samples. **b** The ZFC magnetic moment versus temperature for pure and La samples

(a): The FC magnetic moment versus temperature for pure and La samples

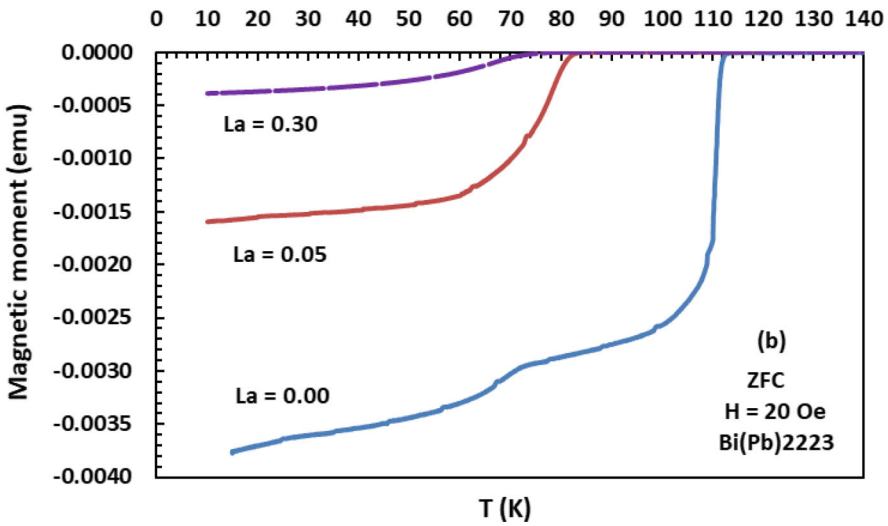

(b): The ZFC magnetic moment versus temperature for pure and La samples

Table 2 T_c, T_c^{mf}, T_{01}, T_{02}, J, $\xi_c(0)$, and OPD versus La for Bi(Pb):2223 system

La cont.	T_c^{mf} (K)	T_{o1} (K)	T_{o2} (K)	J	$\xi_c(0)$ (Å)	λ_1 (R_I)	λ_2 (R_{II})	λ_3 (R_{III})
0.00	124.5	176	132	0.64	7.34	0.30	0.75	0.51
						3D	2D	3D
0.05	111	165	122	0.60	7.12	0.50	0.44	0.99
						3D	3D	2D
0.15	98.5	160	110	0.58	7.02	0.20	0.65	0.38
						3D	2D	3D
0.30	62.5	99.7	74	0.52	6.66	2.04	0.36	0.65
						0D	3D	2D

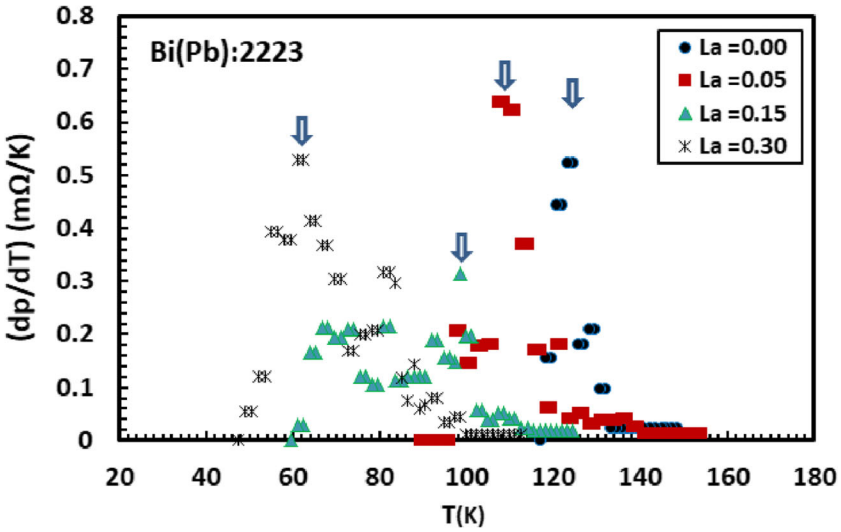

Fig. 4 dρ/dT versus temperature for the pure and La samples

In order to compare the experimental data with the theoretical predictions, these regions are individually linearly fitted, and the values of dimension exponent λ are well determined. However, the first exponent occurs in the normal field region (NFR) at a temperature range of $0.332 \geq \ln\varepsilon \geq -0.883$ for La = 0.00, $0.532 \geq \ln\varepsilon \geq -0.721$ for La = 0.05, $0.711 \geq \ln\varepsilon \geq -0.463$ for La = 0.15, and $1.331 \geq \ln\varepsilon \geq -518$ for La = 0.30. The values of exponents are 0.30 (3D), 0.50 (3D), 0.20 (3D), and 2.04 (0D), respectively. These values indicate that the OD is shifted from 3D to 0D as La increases up to 0.30. The second exponent occurs in the mean field region (MFR) at a temperature range of $-0.907 \geq \ln\varepsilon \geq -1.123$ for = La = 0.00, $-0.739 \geq \ln\varepsilon \geq -2.312$ for La = 0.05, $-0.471 \geq \ln\varepsilon \geq -1.951$ for La = 0.15, and $-0.552 \geq \ln\varepsilon \geq -1.693$ for La = 0.30.The values of exponent are 0.75 (2D), 0.44 (3D), 0.65 (2D), and 0.36 (3D), respectively. The third exponent occurs in the critical field region (CFR) at a temperature range of $-2.809 \geq \ln\varepsilon \geq -4.601$ for = La = 0.00, $-2.432 \geq \ln\varepsilon \geq -4.30$) for La = 0.05, $-2.064 \geq \ln\varepsilon \geq -3.268$ for La = 0.15, and $-1.833 \geq \ln\varepsilon \geq -3.817$ for La = 0.30. The values of exponents are 0.51 (3D), 0.99 (2D), 0.38 (3D), and 0.65 (2D), respectively. This means that the OPD is generally (3D/0D) in the NFR, (2D/ 3D) in the MFR, and (2D/3D) in the CFR.

The appearance 0D in the NFR for La = 030 sample may be due to short wavelength of critical fluctuations in the conductivity region of microscopic granular superconductor, and it is extremely sensible to applied magnetic field as obtained in the diamagnetic measurements [24, 28, 29]. Our interesting point here is observed for the third values of exponents, where the order parameter is shifted from 2D to 3D for La = 0.00 and 0.15 samples, and from 3D to 2D for La = 0.05 and 0.30 samples. This is may be related to the effective length in the direction perpendicular to the current flow which is found to be more reduced in RE^{3+} substituted Bi(Pb):2223 system [50]. This is because most of pure BSCCO systems are 2D behavior in the CFR, and normally the crossover occurs from 3D to 2D

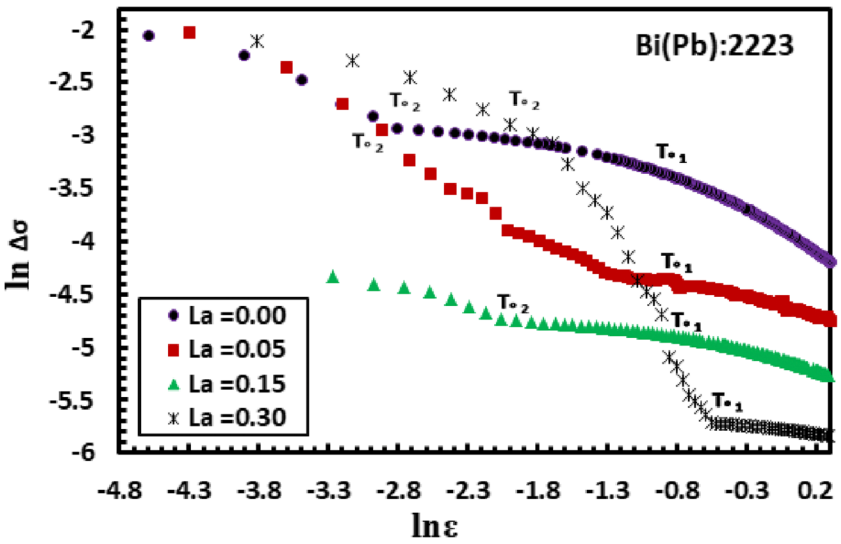

Fig. 5 LnΔσ against lnε for pure and La samples

due to the effect of either substitution or radiation. But at present, the crossover is observed from 3D to 2D and also from 3D to 2D. Actually, the CFR is usually controlled by the critical fluctuation results from the small mean free path of the charge carriers produced as the carrier concentration is changed [23, 51–53]. Our strange point here is that the crossover is not systematic as compared with the increase of La content, which is clearly difficult for understanding.

The anisotropy parameter could be obtained using the relation [54]

$$\gamma = \left[\frac{0.71K_B}{\sqrt{N_G}H_c^2(0)\xi_c^3(0)}\right]^{\frac{1}{2}} = \frac{\xi_{ab}(0)}{\xi_c(0)} \tag{3}$$

N_G is Ginzburg reduced number given by $N_G = \frac{T_{02}-T_{cR}}{T_{cR}}$, and $H_c(0)$ is the thermodynamic critical field at 0 K given by $H_c(0) = \frac{\varphi_0}{2\sqrt{2}\pi\lambda(0)\xi_c(0)}$, where φ_0 is the quantum flux given by $\varphi_0 = \frac{h}{2e} = 2.07 \times 10^{-15}(\mathrm{web/m^2})$, and λ is London penetration depth at 0 K which is about 300 nm for Bi(Pb):2223 superconductors [55]. From the values of γ, the in-plane coherence length $\xi_{ab}(0)$ and effective coherence length $\xi_p(0)$ are obtained with the help of the following relation [12]:

$$\frac{1}{\xi_p(0)} = \frac{1}{4}\left[\frac{1}{\xi_c(0)} + \left(\frac{1}{\xi_c^2(0)} + \frac{8}{\xi_{ab}^2(0)}\right)^{\frac{1}{2}}\right] \tag{4}$$

The upper critical fields at 0 K along the c-axis $H_{c21}(c-\text{axis})$ and along a-b plane $H_{c21}(ab-\text{plane})$, and also the critical current density at 0 K and $J_{c1}(0)$ are calculated by using the following relations [44, 56]:

$$H_{c21}(c\text{–axis}) = \frac{\varphi_0}{2\pi\xi_{ab}^2(0)}$$

$$H_{c21}(ab\text{–plane}) = \frac{\varphi_0}{2\pi\xi_c(0)\xi_{ab}(0)}$$

$$H_{c21}(0) = \sqrt{[H_{c21}(ab\text{–plane})]^2 + [H_{c21}(c\text{–axis})]^2}$$

$$J_{c1}(0) = \frac{2\varphi_0}{\sqrt{6}\pi\lambda^2(0)\xi_p(0)} \tag{5}$$

On the other hand, the lower critical field $H_{c1}(0)$, upper critical fields $H_{c2}(0)$, and also current density at 0 K are estimated by the another following relations [57–60]:

$$H_c(0) = \frac{\varphi_0}{2\sqrt{2}\pi\lambda(0)\xi_c(0)}; H_{c1}(0) = \frac{H_c(0)\ln\kappa}{\sqrt{2}\kappa}$$

$$H_{c22}(0) = \sqrt{2}\kappa H_c(0); J_{c2}(0) = \frac{4\kappa H_{c1}(0)}{3\sqrt{3}\lambda(0)\ln\kappa} \tag{6}$$

where κ is the Ginzburg-Landau parameter of the superconducting system given by $\kappa = \frac{\lambda(0)}{\xi_c(0)}$. As listed in Tables 3 and 4, the values of $\xi_{ab}(0)$, $\xi_p(0)$, and γ are decreased as La increases up to 0.30 as well as both of c-axis, d, J, $\xi_c(0)$, and T_{cR}, while the values of N_G, κ, critical fields, and critical currents are gradually increased. Interestingly, the values of critical fields and critical current obtained from Eq. 5 are approximately higher than those obtained by Eq. 6 (see Fig. 6a, b). Although the above two equations have been used individually, the main reason for the difference between them is not clear for us. On the light of these observations, one can say that the increase of excess oxygen and hole carries/Cu ions introduced by La in the CuO_2 planes of the Bi(Pb):2223 may affect the path of current flow in the system and eventually the critical parameters are increased. This leads to electronic or chemical inhomogeneity in the charge reservoir layer (BiO/SrO) and supplies the charge carriers to the CuO_2 planes through which the actual super-current is believed to flow [61–63].

The order of thermal fluctuations in a superconductor is given by Ginzburg number G_i as follows [64, 65]:

$$G_i = \left[\frac{\pi\kappa^2\xi_0(c)K_BT_c\mu_0}{2\varphi_0^2}\right]^2 \tag{7}$$

where $\mu_0 = 4\pi \times 10^{-7}$ A/m. The G_i values listed in Table 4 are decreased from 8.7×10^{-3} for pure sample to 7×10^{-3}, 3.2×10^{-3}, and 2.1×10^{-3} for La substituted samples. These values are comparable with the reported $G_i = (10^{-3}–10^{-4})$ for HTSC, and they are several orders of magnitude larger than 10^{-9} for conventional superconductor [66, 67]. Decreasing the values of G_i supports the decrease of critical temperature and also the crossover of order parameter dimensionality from 2D/3D or 3D/2D as La increases.

The FTIR absorption spectra of the samples are shown in Fig. 7 and the associated wave numbers for the obtained absorption peaks are listed in Table 5. Regarding the pure sample, the presence of broad absorption peak at 3851.20 cm^{-1} and specific peak at 3493.25 cm^{-1} corresponds to the stretching vibration of intermolecular hydrogen band (O-H), indicating the assignment of fundamental stretching of the OH groups [68, 69]. The appearance of peak band at 1633.36 cm^{-1} is the confirmation of the complex formation of Bi(Pb):2223 phase, in agreement with the report elsewhere [70, 71]. There is a weak and broad absorption peak at 1379.14 cm^{-1}, which may appear due to the presence of small amount of residual carbon. The two successive peaks' appearance at 1184.14 cm^{-1} and 1110.95 cm^{-1} confirms the bond stretching of other metal oxides and carbonates such as $SrCo_3$, $CaCo_3$, and CuO [72–74]. The observed strong peaks at around 586.45 cm^{-1}, 563.28 cm^{-1}, and 532.67 cm^{-1} may be attributed to the characteristic of (metal oxide) O-M vibrations. However, with La substitution, the wave number of few peaks is shifted from its position such as 3493.25 cm^{-1} which is decreased to 3429.77 cm^{-1} and 3436.72 cm^{-1} for La = 0.05

Table 3 N_G, γ, ξ_{ab}, ξ_p, $H_{c\text{-}axis}(0)$, $H_{ab\text{-}plane}(0)$, and $J_c(0)$ versus La for the samples

La cont.	N_G	γ	ξ_{ab} (Å)	ξ_p (Å)	$H_{c21}(0)$ (c-axis) (T)	$H_{c21}(0)$ (ab-plane) (T)	$H_{c21}(0)$
0.00	0.109	0.448	3.29	3.97	3040.82	1362.69	3332.19
0.05	0.173	0.393	2.80	3.45	4196.90	1650.85	4509.91
0.15	0.549	0.357	2.51	3.12	5246.13	1872.70	5570.36
0.30	0.396	0.309	2.06	2.61	7779.30	2404.91	8142.55

and 0.15 samples and then increased to 3493.25 cm^{-1} for La = 0.30. The vice is versa for 1379.14 cm^{-1} band, while the M-O absorption peaks are generally shifted to higher values. Furthermore, the peaks obtained at 1184.14 cm^{-1} and 1110.95 cm^{-1} remain constant for La = 0.05 and 0.15, but they are increased to 1190.14 cm^{-1} and 1132.57 cm^{-1} for La = 0.30 sample.

Anyhow, the FTIR spectra of BSCCO superconductors reflect the contributions of electronic response of the charge carriers and lattice vibrations. The FTIR spectra show different active modes which can be shifted to another wave number by changing either excess oxygen or carrier concentration [4, 33, 75]. The nature of substitutions in BSCCO is considerably simplified by involving the excess oxygen O_δ which makes several predictions that can be easily tested against the observed FTIR spectra [76]. In a marginally stable elastic network, equilibrium conditions require approximate equality of local atomic forces [77]. The highest frequency ω_D of an O–O defects pair scales with its reduced mass μ_D against the reduced mass of the host Cu–O LO mode, μ_H. Thus, $\mu_D\omega_D^2 = \mu_H\omega_H^2$ and with M (Cu) = 4 M (O), $\omega_D = 1.26\ \omega_H$. The maximum LO neutron peak energy is ~ 75 meV = 600 cm^{-1} in BSCCO, in agreement with the present data (586.45 cm^{-1}).

However, the fluctuation-induced excess conductivity study for the pure and La substituted Bi(Pb):2223 phase is considered by the following points: (i) decreasing the values of T_c^{mf} and T_o as well as T_c; (ii) appearance of three different exponents corresponding to two crossover temperatures; (iii) decreasing the coherence lengths, interlayer coupling, G-L parameter, and anisotropy; (v) increasing the Ginzburg number, critical magnetic fields, and critical current. This is due to some reasons such as decreasing c-lattice parameter even La^{3+} ionic size is higher than that of Ca^{2+} at the same eightfold coordination and increasing the excess oxygen and hole carrier concentration per Cu ion. The consistency of these points gives a fair degree of certainty to the appearance of the fluctuation-induced excess conductivity of La substitution in Bi(Pb):2223 system. To our knowledge, the analysis of fluctuation-induced conductivity for the La substituted at Ca site in Bi(Pb):2223 may be considered for the first time and also improves the diamagnetic onset temperature for La = 0.30 sample, which highlight the present work.

4 Conclusion

Fluctuation, diamagnetic, and FTIR in pure and La substituted Bi(Pb):2223 superconductor are investigated. We have shown negative values of magnetic moment below the diamagnetic transition for all samples in both field cooling (FC) and zero-field cooling (ZFC), but the values of FC are higher than those of ZFC. Furthermore, the onset diamagnetic temperature (T_{cM}) for La = 0.30 sample is 83 K, which is about 30 K higher than that obtained from resistivity (T_{cR} = 53 K). On the other hand, the logarithmic plots between $\Delta\sigma$ and ε reveal three different exponents corresponding to two crossover temperatures for all samples. The first exponent occurs in the normal field region (NFR) and its values are 0.30 (3D), 0.50 (3D), 0.20 (3D), and 2.04 (0D). The second exponent occurs in the mean field region (MFR) and its values are 0.75(2D), 0.44 (3D), 0.65 (2D), and 0.36 (3D). The third exponent occurs in the critical field region (CFR) and its values are 0.51 (3D), 0.99 (2D), 0.38 (3D), and 0.65 (2D). Although the substitution of Ca^{2+} by La^{3+} could increase the Ginzburg-Landau parameter, critical magnetic fields, and critical current density, the interlayer coupling, coherence lengths, anisotropy, and Ginzburg number are decreased. Finally, nine successive FTIR absorption

Table 4 k, $H_c(0)$, $H_{c1}(0)$, $H_{c2}(0)$, $J_c(0)$, and G_i versus La for the samples

La cont.	$J_{c1}(0)$ (A/m^2)	κ	$H_c(0)$ (T)	$H_{c1}(0)$ (T)	$H_{c22}(0)$ (T)	$J_{c2}(0)$ (A/m^2)	G_i
0.00	1.17E + 7	408.52	1.057	0.0110	610.67	2.30E + 6	0.0087
0.05	1.45E + 7	421.27	1.089	0.0111	649.36	2.37E + 6	0.0070
0.15	2.46E + 7	427.43	1.106	0.0112	668.49	2.41E + 6	0.0032
0.30	3.64E + 7	450.76	1.166	0.0113	743.46	2.54E + 6	0.0021

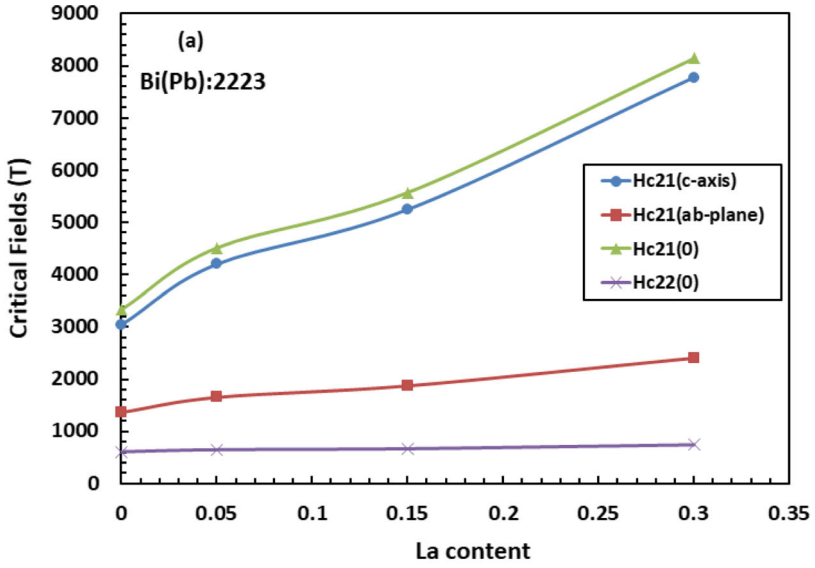

(a): Critical fields versus La content for the samples

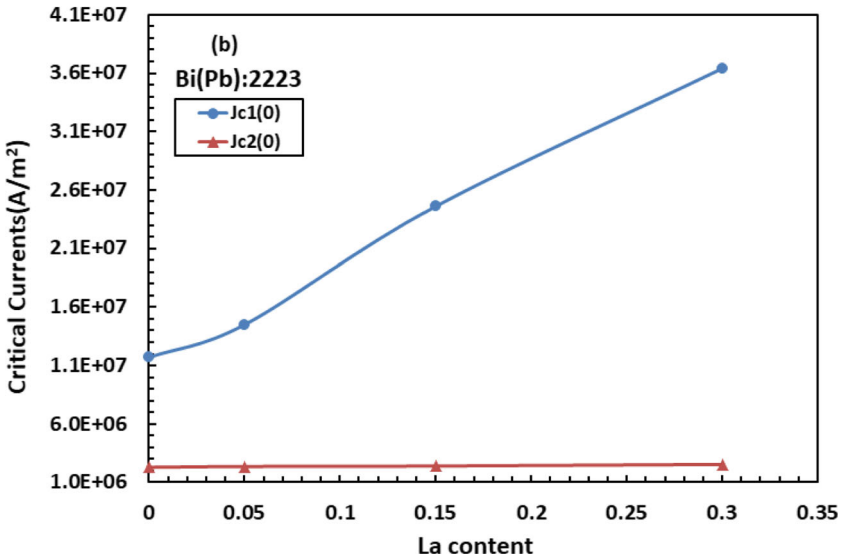

(b): Critical currents versus La content for the samples

Fig. 6 **a** Critical fields versus La content for the samples. **b** Critical currents versus La content for the samples

Table 5 The FTIR spectra for pure and La samples

La cont.	0.00	0.05	0.15	0.30
O-H	3851.20 cm^{-1}	3851.20 cm^{-1}	3851.43 cm^{-1}	3851.20 cm^{-1}
O-H	3493.25 cm^{-1}	3429.77 cm^{-1}	3436.72 cm^{-1}	3493.25 cm^{-1}
Bi(Pb):2223	1633.36 cm^{-1}	1633.36 cm^{-1}	1633.36 cm^{-1}	1633.36 cm^{-1}
Residual carbon	1379.14 cm^{-1}	1427.38 cm^{-1}	1412.04 cm^{-1}	1360.28 cm^{-1}
SrCo	1184.14 cm^{-1}	1184.14 cm^{-1}	1184.14 cm^{-1}	1190.14 cm^{-1}
$CaCo_3$, CuO	1110.95 cm^{-1}	1110.95 cm^{-1}	1110.95 cm^{-1}	1132.57 cm^{-1}
M-O	586.45 cm^{-1}	589.46 cm^{-1}	593.48 cm^{-1}	592.68 cm^{-1}
M-O	563.28 cm^{-1}	563.28 cm^{-1}	582.08 cm^{-1}	574.07 cm^{-1}
M-O	532.67 cm^{-1}	532.67 cm^{-1}	539.33 cm^{-1}	532.67 cm^{-1}

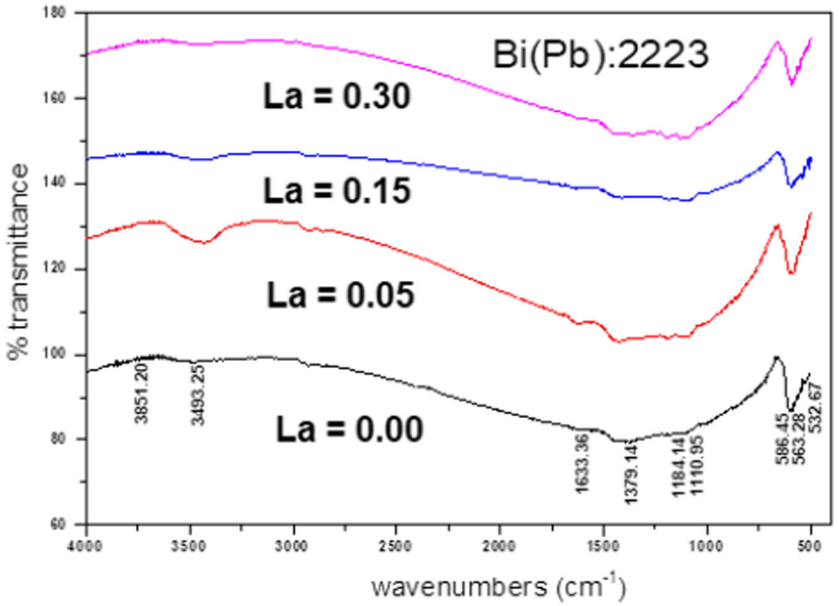

Figure 7 The FTIR absorption spectra of the samples

peaks due to O-H, Bi(Pb):2223, residual carbon, SrCo, $CaCo_3$ and CuO, and M-O could be obtained for all samples. These results are discussed in terms of the balance between hole carriers/Cu ion and excess oxygen which are introduced by La through CuO_2 planes of BSCCO superconductors.

Acknowledgments The authors would like to thank Dr. Mahmoud Abdel-Hafiez, Harvard University, for his cooperation during SQUID measurements.

References

1. Cimberle, M.R., Ferdeghini, C., Giannini, E., Marre, D., Putti, M., Siri, A., Federici, F., Varlomov, A.: Phys. Rev. B. **55**, 14745 (1997)
2. Harabor, A., Harabor, N.A., Deletter, M.: J. Optoelectron. Adv. M. **8**, 1072 (2006)
3. Maeda, H., Tanaka, Y., Fukutomi, M., Asano, T.: Jpn. J. Appl. Phys. **27**(2), L209 (1988)
4. Talantsev, E.F., Strickland, N.M., Hoefakker, P., Xia, J.A., Long, N.J.: Curr. Appl. Phys. **8**, 388 (2008)
5. Hassan, N., Khan, N.A.: J. Appl. Phys. **104**, 103902 (2008)
6. Giannini, E., Gladyshevskii, R., Clayton, N., Musolino, N., Garnier, V., Piriou, A., Flükiger, R.: Curr. Appl. Phys. **8**, 115 (2008)
7. Haraguchi, T., Takayama, S., Kiuchi, M., Otabe, E.S., Matsushita, T., Yasuda, T., Okayasu, S., Uchida, S., Shimoyama, J., Kishio, K.: Physica C (445–448). **123**, (2006)
8. Gheorghe, D.G., Menghini, M., Wijngaarden, R.J., Raedts, S., Silhanek, A.V., Moshchalkov, V.V.: Physica C (437–438). **6**, (2006)
9. Bahrs, S., Bruchhausen, A., Goñi, A.R., Nieva, G., Fainstein, A., Fleischer, K., Richter, W., Thomsen, C.: J. Phys. Chem. Solids. **67**, 340 (2006)
10. Ghosh, A.K., Bandyopadhyay, S.K., Barat, P., Sen, P., Basu, A.N.: Physica C. **255**, 319 (1995)
11. Ghosh, A.K., Basu, A.N.: Supercond. Sci. Technol. **13**, 343 (2000)
12. Khan, N.A., Hassan, N., Nawaz, S., Shabbir, B., Khan, S., Rizvi, A.A.: J. Appl. Phys. **107**, 083910 (2010)
13. Ghosh, A.K., Bandyopadhyay, S.K., Basu, A.N.: Mod. Phys. Lett. B. **11**, 1013 (1997)
14. Fisher, D.S., Fisher, M.P.A., Huse, D.A.: Phys. Rev. B. **43**, 130 (1991)
15. Vidal, F., Veira, J.A., Maja, J., Ponte, J.J., Alvarado, F.G., Mordan, E., Amador, J., Cascales, C.: Physica C. **156**, 807 (1988)
16. Mumtaz, M., Hasnian, S.M., Khurram, A.A., Khan, N.A.: J. Appl. Phys. **109**, 023906 (2011)
17. Esmaeili, A., Sedghi, H., Amniat-Talab, M., Talebian, M.: Eur. Phys. J. B. **79**, 443 (2011)
18. Semba, K., Matsuta, A., Ishii, T.: Phys. Rev. **B49**, 10043 (1994)
19. Mandal, P., Poddar, A., Das, A.N., Ghosh, B., Choudhary, P.: Physica C. **169**, 43 (1990)
20. Wnuk, J.J., Schreurs, L.W.M., Eggenkamp, P.J.T., Van Der Linden: Physica B. **165–166**, 1317 (1990)
21. Mun, M.O., Lee, S.I., Salk, S.H.S., Shin, H.J., Joo, M.K.: Phys. Rev. B. **48**, 6703 (1993)
22. Poddar, A., Mandal, P., Das, A.N., Ghosh, B., Choudhary, P.: Physica C. **161**, 567 (1989)
23. Mori, N., Wilson, J.A., Ozaki, H.: Phys. Rev. **45**, 10633 (1992)
24. Jurelo, A.R., Kunzler, J.V., Schaf, J., Pureur, P.: Phys.Rev.B. **56**(22), 14815 (1997)
25. Schnelle, W., Braun, E., Broicher, H., Weiss, H., Geus, H., Ruppel, S., Galffy, M., Braunisch, W., Waldorf, A., Seidler, F., Wohlleben: Physica C. **161**, 123 (1989)
26. Balestrino, G., Nigro, A., Vaglio, R.: Phys. Rev. **B39**, 12264 (1989)
27. Veira, J.A., Vidal, F.: Phys. Rev. **B42**, 8743 (1990)
28. Khalil, S.M.: J. Low Temp. Phys. **143**(1–2), 31 (2006)
29. Mishra, D.R.: Pranama J. Phys. **70**(3), 535 (2008)
30. Sedky, A., Salah, A., Amin, S.A.: Asian J. Phys. Sci. Chem. 3,2,1 (2017)
31. Sale, F.R., Mahloojchi, F.: Ceram. Int. **14**, 229 (1988)
32. Yanru, R., Hanpeng, L., Mingzhu, L., Qingyun, T., Lihua, S., Zhenjin, L., Xianren, M.: Physica 156. **5**, 799 (1988)
33. Hwang, J., Timusk, T., Gu, G.D.: Nature. **427**, 714 (2004)
34. Norman, M.: Nature. **427**, 692 (2004)

35. Sedky, A., Salah, A., Bahgat, A.A., Abou-Aly, A.: J. Mater. Sci. Mater. Electron. **31**(15), 12502 (2020)
36. Galluzzi, A., Polichetti, M., Buchkov, K., Nazarova, E., Mancusi, D., Pace, S.: Supercond. Sci. Technol. **28**, 115005 (2015)
37. Maheshwari, P.K., Jha, R., Gahtori, B., Awana, V.P.S.: AIP Adv. **5**, 097112 (2015)
38. dos Santos, A.D.M., Moehlecke, S., Kopelevich, Y., Machado, A.J.S.: Physica C. **390**, 21 (2003)
39. Ovchnnikov, Y.N., Wolf, S.A., Kresin, V.Z.: Phys. Rev. B. **63**, 064524 (2001)
40. Das, A., Suryanarayanan, R.: Aust. J. Phys. **15**, 623 (1995)
41. Anderson, W., Zou, Z.: Phys. Rev. Lett. **60**, 132 (1988)
42. Aslamazov, L.G., Larkin, A.I.: Phys. Lett. A. **26**, 238 (1968) Sov. Phys. Solid state 10, 875 (1968)
43. Lawrence, W.E. and Doniach, S., Proc, S.: 12th Int. Conf. Low Temp. Phys. Kyoto, 1970 (Edited by E. Kanada), P. 361, Keigaku, Tokyo (1971)
44. Gosh, A.K., Bandyopadhyay, S.K., Basu, A.N.: J. Appl. Phys. **86**, 3247 (1999)
45. Sedky, A.: J. Low Temp. Phys. **148**, 53 (2007)
46. Ramallo, M.V., Torron, C., Vidal, F.: Physica C. 230.97 (1994)
47. Baraduc, C., Bazdin, A.: Phys. Lett. A. **171**, 408 (1992)
48. Reggiani, L., Vaglio, R., Varlamo, A.A.: Phys. Rev. B. **44**, 9541 (1991)
49. Mandal, P., Poddar, A., Das, A.N.: J. Phys. Condens. Matter. **6**, 5689 (1994)
50. Roumié, M., Abdeen, R., Awad, R., Korek, M., Hassan, I., Mawassi, R.: J. Low Temp. Phys. **174**, 45 (2014)
51. Sedky, A., Al-Battat, W.: Phys. B. **410**, 227 (2013)
52. Ravi, S., Seshu Bai, V.: Solid State Commun. **83**, 117 (1992)
53. Veira, J.A., Maza, J., Vida, J.: Phys. Lett.A. **131**, 310 (1988)
54. Petrovie, A., Fasano, Y., Lortz, R., Decrouc, M., Potel, M., Chevrel, R., Fischer, O.: Physica C. **460–462**, 702 (2007)
55. Sedky, A.: J. Magnetism Mag. Mater. **277**, 293 (2004)
56. Petrovie, Y., Fasano, R., Lortz, M., Dcrous, M., Potel, M., Cheriel, R.: Physica C. **460–462**, 702 (2007)
57. Abou-Aly, A.I., Awad, R., Kamal, M., Anas, M.: J. Low Temp. Phys. **163**, 184 (2011)
58. Poole, P.C., Farach, A.H., Creswick, J.R., Prozorov, R.: Superconductivity, 2nd edn. Academic Press, Elsevier, San Diego (2007)
59. Abou Aly, A.I., Ibrahim, I.H., Awad, R., El-Harizy, A., Khalaf, A.: J. Supercond. Nov. Magn. **23**(7), 1325 (2010)
60. Abou-Aly, A.I., Awad, R., Ibrahim, I.H., Abdeen, W.: Solid State Commun. **140**, 281 (2009)
61. Aloysius, R.P., Guruswamy, P., Syamaprasad, U.: Supercond. Sci. Technol. **18**, L1 (2005)
62. Biju, A., Sarun, P.M., Aloysius, R.P., Syamaprasad, U.: Mater. Res. Bull. **42**, 2057 (2007)
63. Biju, A., Sarun, P.M., Aloysius, R.P., Syamaprasad, U.: J. Alloys Compound. **431**, 49 (2007)
64. Jaroszynski, J., Riggs, S.C., Hunte, F., Gurevich, A., Larbalestier, D.C., Boebinger, G.S., Balakirev, F.F., Migliori, A., Ren, Z.A., Lu, W., Yang, J., Shen, X.L., Dong, X.L., Zhao, Z.X., Jin, R., Sefat, A.S., McGuire, M.A., Sales, B.C., Christen, D.K., Mandrus, D.: Phys. Rev. B. **78**, 064511 (2008)
65. Mun, M.O., Lee, S.I., Lee, W.C.: Phys. Rev. B. **56**, 14668 (1997)
66. Pribulova, Z., Klein, T., Kacmarcik, J., Marcenat, C., Konczykowski, M., Bud'ko, S.L., Tillman, M., Canfield, P.C.: Phys. Rev. B. **79**, 020508 (2009)
67. Kim, S., Choi, C., Jung, M., Yoon, J., Jo, Y., Wang, X., Chen, X., Wang, X.L., Lee, S., Choi, K.: J. Appl. Phys. **108**(6), 063916 (2010)
68. Arshad, M., Qureshi, A.H., Masud, K., Qazi, N.K.: J. Therm. Anal. Calorim. **89**, 595 (2007)
69. Jamil, S.H., Hashim, A., Yahya, S.Y.S., Kasim, A., Hasan, N.H., Wahab, N.A.: Malays. J. Anal. Sci. **19**(6), 1284 (2015)
70. Alcockand, C.B., Li, B.: J. Am. Ceram. Soc. **73**, 1176 (1990)
71. Selvan, R.K., Augustin, C.O., et al.: Mater. Res. Bull. **200**(38), 41 (2003)
72. Qureshi, A.H., Arshad, M., et al.: J. Therm. Anal. Cal. **81**, 363 (2005)
73. Qureshi, A.H., Durani, S.K., et al.: J. Chem. Soc. Pak. **25**, 177 (2003)
74. Kumar, R., Singh, H.S., Singh, Y.: AIP Conf. Proc. 1953. 030001–1–030001-4 (2017)
75. Hudakova, N., Knizek, K., Hejtmanek, J.: Physica C. **406**, 58 (2004)
76. Xu, G., Qirong, P., Liu, B., Zhang, J., Zhang, C., Ding, Z., Zhang, Y.: Physica C. **390**, 75 (2003)
77. Phillips, J.C.: Phys. Stat. Solid. (B), Appl. Res. **242**(1), 51 (2005)
78. Ghorbani, S.R., Homaei, M.: Modern Phys. Lett. B. **25**(23), 1915 (2011)